Similarity of Wireless Multiband Propagation in Urban Vehicular-to-Infrastructure Scenarios

Markus Hofer*, David Löschenbrand*, Faruk Pasic[†], Danilo Radovic[†], Benjamin Rainer*, Jiri Blumenstein[⊕], Christoph F. Mecklenbräuker[†], Seun Sangodoyin[⋄], Hussein Hammoud[‡], Gerald Matz[†], Andreas F. Molisch[‡] and Thomas Zemen*

*AIT Austrian Institute of Technology GmbH, Austria

†Institute of Telecommunications, TU Wien, Vienna, Austria

†Dept. of Radio Electronics, Brno University of Technology, Czech Republic

†Georgia Institute of Technology, Atlanta, GA, USA

†University of Southern California, Los Angeles, CA, USA

Abstract—Cooperative connected automated mobility depends on sensing and wireless communication functions. With increasing carrier frequency both functions can be realized with the same hardware, however, the attenuation of radio signals increases quadratically with the carrier frequency. Hence, link setup becomes challenging in vehicular scenarios due to the required beam finding process. In this paper we investigate the multipath components of the vehicle-to-infrastructure (V2I) radio channel in three frequency bands with center frequencies of 3.2 GHz, 34.3 GHz and 62.35 GHz using measurement data with 155.5 MHz bandwidth and a sounding repetition rate of 31.25 μ s. The channel impulse responses are collected simultaneously at all three carrier frequencies. Using the high temporal sampling rate we apply the CLEAN algorithm, enabling the estimation of the weight, delay and Doppler frequency of multipath components. By analyzing the collinearity of the Doppler normalized scattering function between the frequency bands we found that the collinearity between the 3.2 GHz and 34.3 GHz band as well as between the 3.2 GHz and 62.35 GHz is smaller in the non-line of sight (NLOS) region but increases for the line-of-sight (LOS).

Index Terms—multiband, mmWave, wireless channel measurements, wireless channel sounding, software defined radio

I. INTRODUCTION

Cooperative connected automated mobility relies on exchanging sensor data and traffic status information with other road users and the infrastructure. The utilization of the millimeter wave (mmWave) frequency bands enables an increased bandwidth and the use of a single radio interface for sensing and communication function. However, the high radio signal attenuation requires beamforming which is challenging in vehicular scenarios. At high-velocities, the beam direction finding may take up a significant portion of the channel stationarity interval, leaving insufficient time for link utilization. Therefore, it is necessary to discover alternative methods to reduce the training overhead in order to maximize the achievable data rate.

A possible solution to reduce the overhead is to utilize information acquired in another frequency band to aid the link configuration in the mmWave band [1]. Although sub6 GHz bands typically allow for less bandwidth, they provide more favorable propagation conditions, in particular showing a lower isotropic free-space pathloss, and better blockage resilience. Several recent multiband measurement campaigns show that mmWave frequency bands have similar propagation characteristics as sub-6 GHz frequency bands [2]–[7]. Hence, channel state information of the sub-6 GHz band can aid channel estimation and beamforming in the mmWave band.

The aforementioned papers perform mostly a statistical analysis of similarities between different frequency bands; a detailed path-wise analysis is often missing. To resolve the individual multipath components (MPCs) and to obtain their properties, the CLEAN algorithm, an iterative deconvolution technique initially designed for image enhancement in radio astronomy [8], can be applied.

Several publications [9]–[14] have either utilized or modified the CLEAN algorithm for various purposes. Earlier versions of the CLEAN algorithm such as those introduced in [9] and [10] are used to facilitate spatio-temporal distinction of MPCs in ultrawideband propagation channels. A comparison of two variants of the CLEAN algorithm to estimate MPCs in an intra-vehicular propagation channel is given in [11].

A path parameter estimation algorithm with similarity to CLEAN is proposed in [12]. The sub-grid CLEAN algorithm is proposed in [13] and utilizes a two-step peak search i.e., a global coarse search followed by a fine sub-grid search methodology for MPCs parameter estimation. The refinement to peak estimation in the sub-grid CLEAN improves the accuracy of estimated MPCs. In [14] serial interference cancellation is used to detect scatterers of a radar target in delay and Doppler domain in a serial manner.

Contribution of the paper:

- In this paper we use the CLEAN algorithm to obtain delay, Doppler shift, and path weight of the MPCs within the three measured frequency bands at 3.2 GHz, 34.3 GHz and 62.35 GHz.
- We compare the obtained delays, Doppler shifts, and

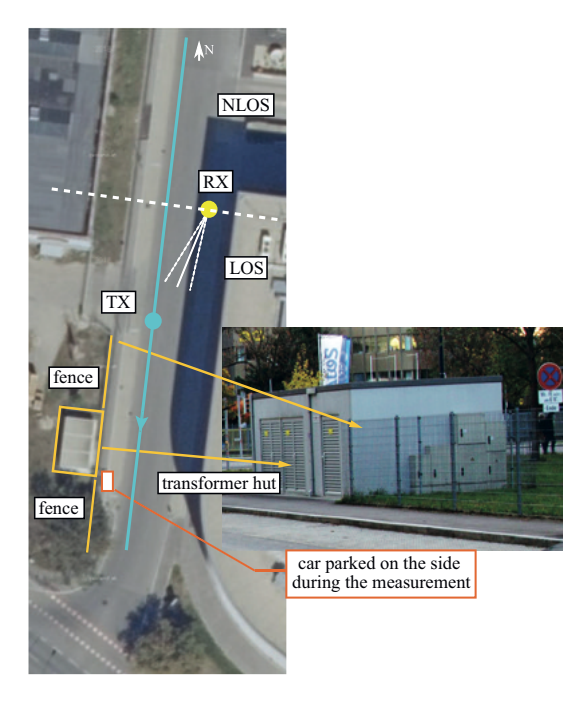


Fig. 1. Overview of the measurement scenario [15]. A TX car approaches a "T"-intersection and stops. The directive RX horn antennas are pointed towards the road intersection. On the right side of the road there is a metallic fence with metallic pillars and a transformer hut [2].

multipath weights between the frequency bands and investigate their similarity by means of the Doppler-adjusted scattering function. The results show that a high similarity can be found between the frequency bands. Finally, we demonstrate the dependency of the evaluated intra-band correlation on the stationarity region length.

II. MEASUREMENT DESCRIPTION

In this paper we utilize the measurement results of a tripleband measurement campaign [2] conducted in an urban V2I scenario shown in Fig. 1 and described briefly here. A transmitter (TX) car that is equipped with three omni-directional antennas (see Fig. 2) passes by a static receiver (RX) (see Fig. 3) with three directive antennas mounted on a tripod and stops at a road intersection. The transmitter trajectory is indicated with cyan color in Fig. 2, the receiver position is indicated a by yellow circle and the orientation of the directive antennas is shown by white color. The directive antennas have a half power beam width of approximately 17-19°. We use an orthogonal frequency division multiplexing based channel sounder [16], [17] to simultaneously obtain the channel transfer function (CTF) at $f_0 = 3.2 \,\text{GHz}$, $f_1 = 34.3 \,\text{GHz}$ and $f_2 = 62.35 \,\text{GHz}$. The sampled time-variant CTF per frequency band is obtained by

$$H[m,q;i] = H(mt_s, qf_s;i), \tag{1}$$

where m indicates the time index, q is the frequency index, $i \in \{0,\ldots,I-1\}$ is the band index, $t_{\rm s}=31.25\,\mu{\rm s}$ the repetition time of the sounding signal and $f_{\rm s}=B/Q$ is the sampling rate in frequency. For these measurements we used

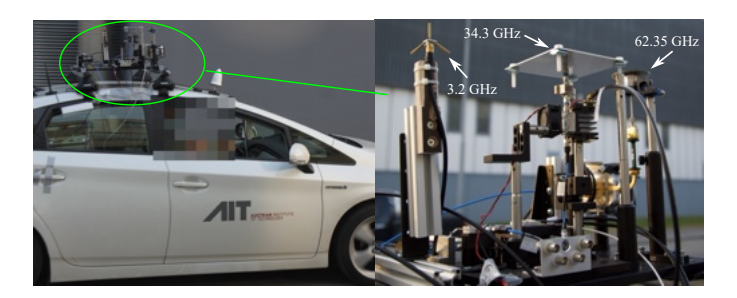


Fig. 2. Transmit antennas mounted on car rooftop [2].

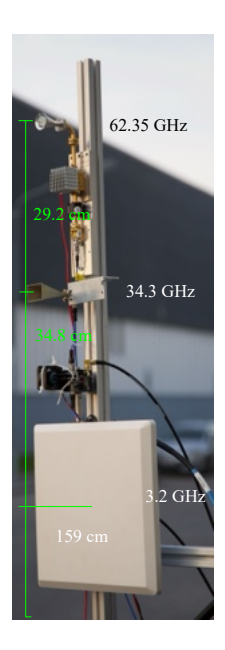


Fig. 3. Receive antennas mounted on a pole of a tripod [2].

a bandwidth $B=155.5\,\mathrm{MHz}$ with Q=311 subcarriers (thus, $f_s=500\,\mathrm{kHz}$). Coordinates of the TX are recorded with a real-time kinematic global positioning system (GPS) receiver. A detailed description of the measurement setup can be found in [2].

III. PARAMETER EVALUATION

To obtain a detailed analysis of the CTF we use the CLEAN algorithm to identify MPCs in each frequency band. We subsequently calculate the collinearity, also called cosine similarity in literature, of the corresponding scattering functions in the three frequency bands.

A. Extending the CLEAN Algorithm

We extend the algorithm from [12] to the delay-Doppler domain, to obtain high resolution estimates of the path delay, Doppler frequency and complex weight of the MPCs in an iterative way. For data evaluation, the time-variant CTF is divided in stationarity regions that are indexed by s and consist of M time samples and of Q frequency samples. We assume that within the stationrity regions the statistics of the fading process do not change significantly [18]–[20]. For notational

simplicity we drop the band index i and assume that the timevariant frequency response $H_s[m,q] = H[m+sM,q]$ within stationarity region s is the sum of P MPCs

$$H_s[m,q] = \sum_{p=1}^{P} \alpha_{s,p} e^{j2\pi y(\theta_{s,p}m - \nu_{s,p}q)},$$
 (2)

where $\alpha_{s,p} \in \mathbb{C}$ is the complex path weight, $\nu_{s,p}$ is the normalized Doppler, and $\theta_{s,p}$ is the normalized delay of the pth path. The CLEAN algorithm proceeds as follows:

- 1) Initialize $H_{s,p}[m,q] = H_s[m,q]$ for stationarity region s of the CTF with p = 1, corresponding to the first MPC.
- 2) Compute the scattering function by a discrete Fourier transform in time and frequency that reads

$$S_{s,p}[n,l] = \frac{1}{MQ} \left| \sum_{m=0}^{M-1} \sum_{q=-Q/2}^{Q/2-1} H_{s,p}[m,q] e^{-j2\pi (\frac{lm}{M} - \frac{nq}{Q})} \right|^2$$
(3)

3) The strongest component in the scattering function is identified as

$$(\hat{n}, \hat{l}) = \underset{(n,l)}{\operatorname{arg\,max}} S_{s,p}[n, l], \tag{4}$$

with delay index $n \in \{0, \dots, Q-1\}$ and Doppler index $l \in \{-M/2, \dots, M/2-1\}$.

4) We define a high resolution grid in delay and Doppler with R equally spaced intervals in both domains, surrounding the strongest multipath component found with (4). This results in R² candidate points for the search grid defined as

$$\frac{\hat{l}-1}{M} \le \nu_u < \frac{\hat{l}+1}{M}, \quad \nu_u = \frac{\hat{l}-1}{M} + u\frac{2}{RM}$$

and

$$\frac{\hat{n}-1}{Q} \le \theta_k < \frac{\hat{n}+1}{Q}, \quad \theta_k = \frac{\hat{n}-1}{Q} + k\frac{2}{RQ},$$

where $u,k \in \{0,\ldots,R-1\}$. We search for the pair (\hat{u},\hat{k}) such that

$$(\hat{u}, \hat{k}) = \underset{0 \le u, k \le R-1}{\arg\max} \left| \sum_{m=0}^{M-1} \sum_{q=-Q/2}^{Q/2-1} \mathrm{e}^{-\mathrm{j}2\pi(\theta_k m - \nu_u q)} \right|$$

$$H_{s,p}[m,q]$$
 (5)

and obtain $\hat{\nu}_{s,p} = \nu_{\hat{u}}$ and $\hat{\theta}_{s,p} = \theta_{\hat{k}}$.

5) Having found the high resolution estimates $(\hat{\nu}_{s,p}, \hat{\theta}_{s,p})$ we subtract the found MPC from the time-variant frequency response sequence for stationarity region s

$$H_{s,p+1}[m,q] = H_{s,p}[m,q] - \hat{\alpha}_{s,p} e^{j2\pi(\hat{\theta}_{s,p}m - \hat{\nu}_{s,p}q)},$$
 (6)

with path weight

$$\hat{\alpha}_{s,p} = \frac{1}{MQ} \left(\sum_{m=0}^{M-1} \sum_{q=-Q/2}^{Q/2-1} e^{-j2\pi(\hat{\theta}_{s,p}m - \hat{\nu}_{s,p}q)} \right)$$

$$H_{s,p}[m,q] . \tag{7}$$

6) Go to step 1) with p = p + 1 and iterate the algorithm until p = P.

B. Cosine Similarity

To enable a direct comparison of the fading processes at the frequencies f_0 , f_1 and f_2 we readjust the Doppler shift of the MPCs detected by the CLEAN algorithm

$$\nu'_{s,p;i} = \hat{\nu}_{s,p;i} f_2 / f_i \,. \tag{8}$$

We compute the time-variant frequency response using (2) and compute the Doppler-adjusted scattering function $S_{s,i}'[n,l]$ using (3). We then calculate the collinearity, also referred to as cosine similarity in literature, per stationarity region [20] among the reconstructed Doppler-adjusted scattering functions according to

$$\rho_{s,i,j} = \frac{\sum_{n=0}^{Q-1} \sum_{l=-M/2}^{M/2-1} \left| S'_{s,i}[n,l] \right| \left| S'_{s,j}[n,l] \right|}{MQ \sqrt{\sigma_{s,i}^2 \sigma_{s,j}^2}}, \quad (9)$$

with the sample variance

$$\sigma_{s,i}^2 = \frac{1}{MQ} \sum_{n=0}^{Q-1} \sum_{l=-M/2}^{M/2-1} \left| S_{s,i}'[n,l] \right|^2.$$
 (10)

IV. Results

In this section we present the results using the algorithms described in Sec. III. We refer the reader to [2] to compare the results with the calculated power delay profile (PDP) and Doppler spectral density (DSD) of the measurement. For the evaluation in this paper we choose R=10, M=3200 (which is equal to a stationarity time $T_{\rm stat}=100\,{\rm ms}$) and calculate the P=20 strongest MPCs. We don't use a stop criterion for the power of the detected MPCs in the evaluation. In Sec. IV-B we evaluate the correlation between the three frequency bands. Furthermore, we show the influence of the selected stationarity time on the correlation between the bands.

A. Multipath Components Obtained by CLEAN

The scatter plots in Fig. 4 and Fig. 5 show the path delays and the Doppler shifts adjusted by (8) for the P=20 strongest MPCs for each frequency band, respectively. The blue color in the plots represents the 3.2 GHz band, the red color the 34.3 GHz band and the orange color the 62.35 GHz band. We indicate by the left black vertical line in the plot the time $t_1=11.6\,\mathrm{s}$ when the TX passes the RX and by the right black vertical line the time $t_2=21\,\mathrm{s}$ when the TX stops at the road intersection. We define the region until t_1 as NLOS region and the region from t_1 onwards as LOS region.

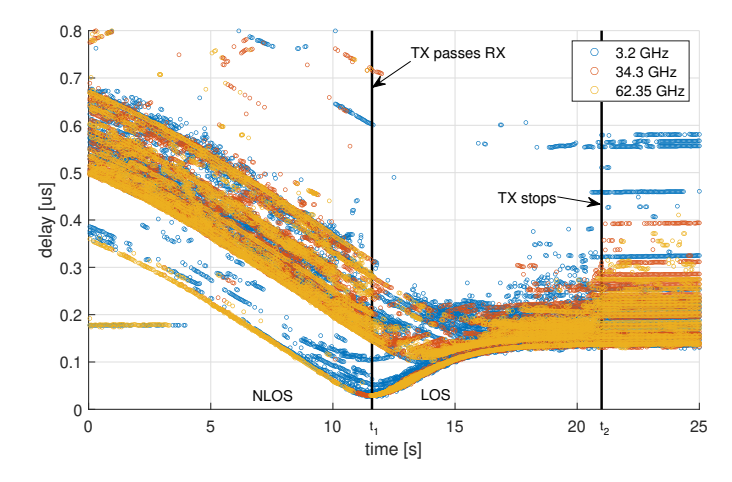


Fig. 4. Delay of multipath components vs. time. The 20 strongest MPCs obtained by the CLEAN algorithm for 3.2 GHz (blue), 34.3 GHz (red) and 62.35 GHz (orange) are shown.

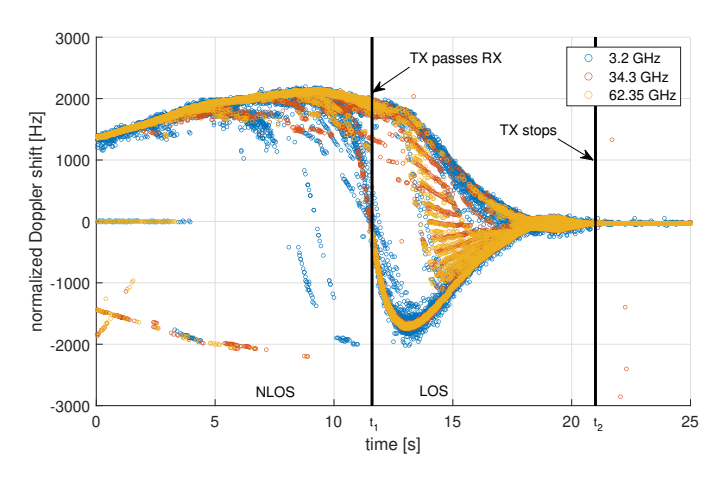


Fig. 5. Adjusted Doppler shift of multipath components vs. time. The P=20 strongest MPCs obtained by the CLEAN algorithm for 3.2 GHz (blue), 34.3 GHz (red) and 62.35 GHz (orange) are shown. The Doppler is adjusted according to (8) to compensate for the linear effect of the different carrier frequencies.

We observe that as the TX approaches the RX the path delays decrease and their Doppler shifts are positive. The moment the TX passes the RX the Doppler shift of the main LOS component becomes negative. The CLEAN algorithm furthermore detects reflected MPCs stemming from fences, lamp posts and a transformer hut on the opposite side of the RX as indicated in Fig. 1.

To obtain a better understanding we show in Fig. 6 a 3D scatter plot of the five strongest MPC (more MPCs lead to reduced clarity in the figure) of each frequency band between t_1 and t_2 . In this plot the y-axis is the Doppler-adjusted frequency, while the z-axis is the path delay. From the plot we see that the delay and the Doppler-adjusted frequency of the LOS component matches in all frequency bands well. Furthermore, the second strongest MPC in the LOS region in all bands stem from a parked car close to the road intersection. Utilizing the recorded GPS coordinates, the geometry of the scenario and the calculated MPCs parameters we further find

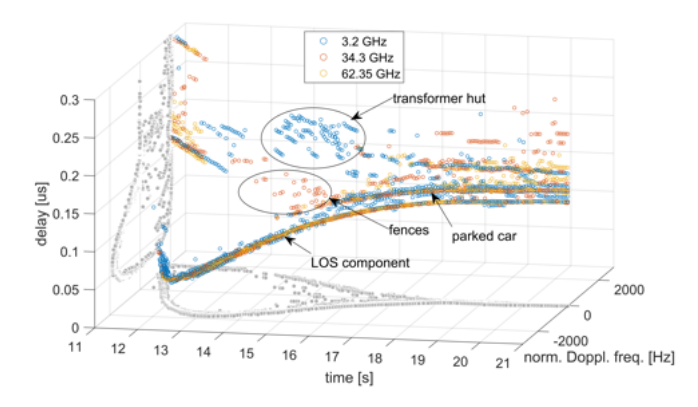


Fig. 6. 3D scatter plot of the 5 strongest MPCs obtained by the CLEAN algorithm between t_1 and t_2 for 3.2 GHz (blue), 34.3 GHz (red), and 62.35 GHz (orange).

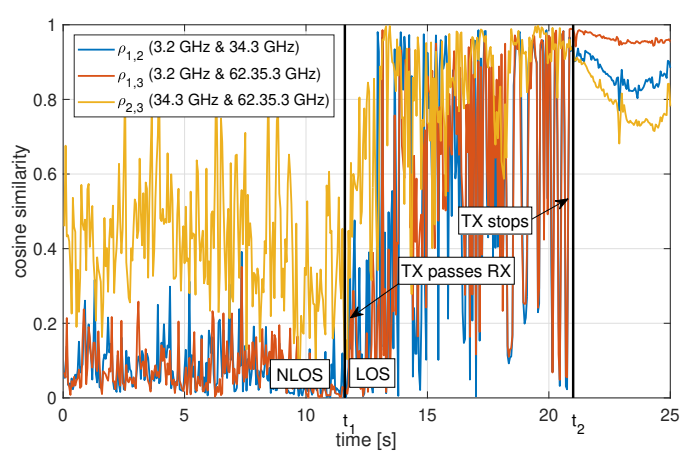


Fig. 7. Cosine similarity $\rho_{i,j}$ of the Doppler-adjusted scattering function for different frequency bands i and j vs. time, see (9).

that several reflections in the mmWave bands 34.3 GHz and 62.35 GHz (i.e., the ladder structure in plot Fig. 5) stem from a fence on the opposite side of the RX. The strongest diffuse reflections in the 3.2 GHz band stem from the transformer hut.

B. Cosine Similarity

We evaluate the cosine similarity according to Sec. III-B. Fig. 7 shows the cosine similarity between the frequency bands vs. time. The blue color shows the cosine similarity $\rho_{1,2}$ between the 3.2 GHz and the 34.3 GHz band, the red color shows the cosine similarity $\rho_{1,3}$ between the 3.2 GHz and the 62.35 GHz band and the orange color shows the cosine similarity $\rho_{2,3}$ between the 34.3 GHz and the 62.35 GHz band. As expected, the cosine similarity in the NLOS region is lower compared to the LOS region. In the LOS region the mean value of the cosine similarity is higher due to the power of the strong LOS component.

Finally we show the empirically calculated cumulative distribution functions (CDFs) of the cosine similarity for the NLOS region in Fig. 8 and for the LOS region in Fig. 9.

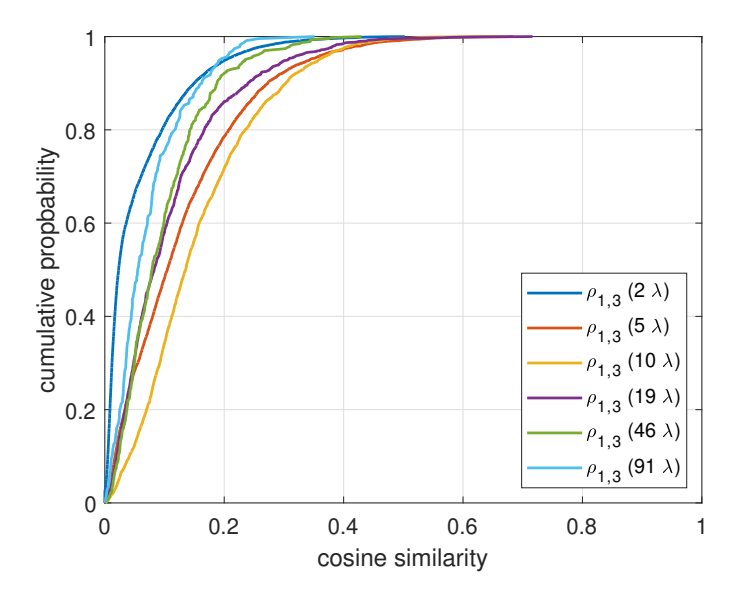


Fig. 8. Empirically calculated CDF of $\rho_{1,3}$ for the NLOS region between 0 and t_1 .

Different stationarity region lengths are shown for the cosine similarity between the 3.2 GHz and the 62.35 GHz band. From the results we observe that the cosine similarity increases with increasing stationarity region length up to a wavelength of approximately 10λ . Here, the wavelength refers to the 62.35 GHz band and is calculated with the average velocity within t_1 and t_2 . This can be explained since with increasing observation length M, the Doppler estimation error decreases. A relation between observation length and Doppler estimation accuracy can be found in [21]. For a stationarity region length of 10λ the cosine similarity is larger than 0.8 for more than 50% of the time and larger than 0.9 for more than 37% of the time. If the stationarity region length is increased above 10λ the cosine similarity decreases again since the stationarity conditions are violated due to vehicular motion. For, e.g., a stationarity region length of 91 λ a cosine similarity larger than 0.8 is only valid for approximately 31 \% of the time and a cosine similarity larger than 0.9 only for approximately 20%of the time.

V. CONCLUSIONS

In this paper we applied the CLEAN algorithm to obtain high resolution estimates of the path delay, Doppler frequency and complex weight of MPCs for the frequency bands 3.2 GHz, 34.3 GHz and 62.35 GHz. Using the results we analyzed the similarities of the frequency bands in an urban V2I measurement scenario and found that the LOS component and the strongest reflected MPC can be clearly observed in all three frequency bands. We furthermore assessed the origin of the reflections in the mmWave bands. By analyzing the cosine similarity between the frequency bands we found that the cosine similarity between the 3.2 GHz and 34.3 GHz band as well as between the 3.2 GHz and 62.35 GHz is smaller in the NLOS region but increases for the LOS region. Finally, we analyzed the cosine similarity depending on the stationarity

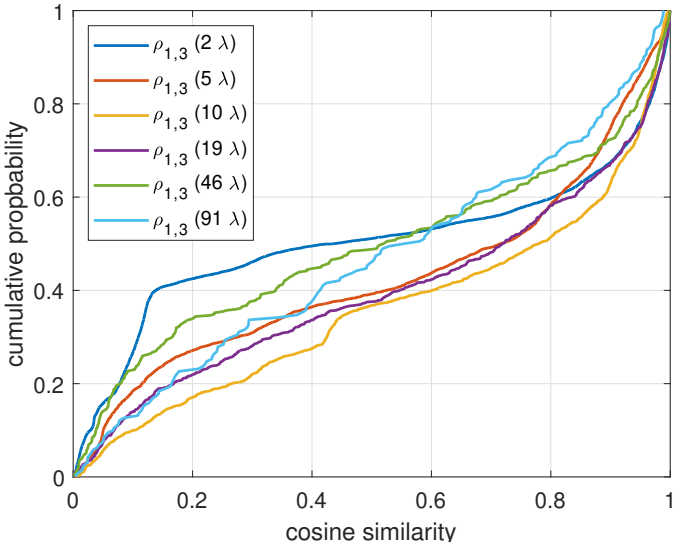


Fig. 9. Empirically calculated CDF of $\rho_{1,3}$ for the LOS region between t_1 and t_2 .

region lengths in terms of wavelength and found that small and very large stationarity region lengths for this scenario lead to reduced cosine similarity results. For short stationarity region length the Doppler resolution is reduced, and for too long stationarity region lengths the assumed stationarity conidtion is violated.

ACKNOWLEDGEMENT

This work was supported in part by the Austrian Research Promotion Agency FFG through the TRITON project (grant agreement No 858697), the project DEDICATE (Principal Scientist grant) at the AIT Austrian Institute of Technology. the COST Action INTERACT, CA20120, supported by COST (European Cooperation in Science and Technology) and the Czech Science Foundation, Project No. 22-04304L, Multiband prediction of millimeter-wave propagation effects for dynamic and fixed scenarios in rugged time varying environments.

The work of H. Hammoud and A. F. Molisch was supported by the National Science Foundation grants 1926913 and 2106602, and the California Transportation Authority under the METRANS program.

REFERENCES

- [1] N. Gonzalez-Prelcic, A. Ali, V. Va, and R. W. Heath, "Millimeter-wave communication with out-of-band information," *IEEE Communications Magazine*, vol. 55, no. 12, pp. 140–146, 2017.
- [2] M. Hofer, D. Löschenbrand, J. Blumenstein, H. Groll, S. Zelenbaba, B. Rainer, L. Bernadó, J. Vychodil, T. Mikulasek, E. Zöchmann, S. Sangodoyin, H. Hammoud, B. Schrenk, R. Langwieser, S. Pratschner, A. Prokes, A. F. Molisch, C. F. Mecklenbräuker, and T. Zemen, "Wireless vehicular multiband measurements in centimeterwave and millimeterwave bands," in 2021 IEEE 32nd Annual International Symposium on Personal, Indoor and Mobile Radio Communications (PIMRC), 2021, pp. 836–841.
- [3] M. Hofer, D. Löschenbrand, S. Zelenbaba, A. Dakić, B. Rainer, and T. Zemen, "Wireless 3 GHz and 30 GHz vehicle-to-vehicle measurements in an urban street scenario," in *IEEE 96th Vehicular Technology Conference (VTC2022-Fall)*, 2022.

- [4] D. Dupleich, R. Müller, M. Landmann, E. Shinwasusin, K. Saito, J. Takada, J. Luo, R. Thomä, and G. Del Galdo, "Multi-band propagation and radio channel characterization in street canyon scenarios for 5G and beyond," *IEEE Access*, vol. 7, pp. 160385–160396, 2019.
- [5] P. Kyösti, P. Zhang, A. Pärssinen, K. Haneda, P. Koivumäki, and W. Fan, "On the feasibility of out-of-band spatial channel information for millimeter-wave beam search," *IEEE Transactions on Antennas and Propagation*, vol. 71, no. 5, pp. 4433–4443, 2023.
- [6] F. Pasic, M. Hofer, M. Mussbah, H. Groll, T. Zemen, S. Schwarz, and C. F. Mecklenbräuker, "Statistical evaluation of delay and Doppler spreads in sub-6 GHz and mmWave vehicular channels," in *IEEE 97th Vehicular Technology Conference (VTC2023-Spring)*, 2023.
- [7] M. Boban, D. Dupleich, N. Iqbal, J. Luo, C. Schneider, R. Müller, Z. Yu, D. Steer, T. Jämsä, J. Li, and R. S. Thomä, "Multi-band vehicleto-vehicle channel characterization in the presence of vehicle blockage," *IEEE Access*, vol. 7, pp. 9724–9735, 2019.
- [8] J. Högbom, "Aperture synthesis with a non-regular distribution of interferometer baselines," Astronomy and Astrophysics Supplement, Vol. 15, p. 417, vol. 15, p. 417, 1974.
- [9] Q. H. Spencer, B. D. Jeffs, M. A. Jensen, and A. L. Swindlehurst, "Modeling the statistical time and angle of arrival characteristics of an indoor multipath channel," *IEEE Journal on Selected areas in communications*, vol. 18, no. 3, pp. 347–360, 2000.
- [10] R.-M. Cramer, R. A. Scholtz, and M. Z. Win, "Evaluation of an ultrawide-band propagation channel," *IEEE Transactions on Antennas and Propagation*, vol. 50, no. 5, pp. 561–570, 2002.
- [11] A. Chandra, J. Blumenstein, T. Mikulasek, J. Vychodil, M. Pospisil, R. Marsalek, A. Prokes, T. Zemen, and C. Mecklenbräuker, "CLEAN algorithms for intra-vehicular time-domain UWB channel sounding," in International Conference on Pervasive and Embedded Computing and Communication Systems (PECCS). IEEE, 2015.
- [12] K. Mahler, W. Keusgen, F. Tufvesson, T. Zemen, and G. Caire, "Tracking of wideband multipath components in a vehicular communication scenario," *IEEE Transactions on Vehicular Technology*, vol. 66, no. 1, pp. 15–25, 2016.
- [13] M. Kim, T. Iwata, S. Sasaki, and J.-I. Takada, "Millimeter-wave radio channel characterization using multi-dimensional sub-grid CLEAN algorithm," *IEICE Transactions on Communications*, vol. 103, no. 7, pp. 767–779, 2020.
- [14] N. K. Nataraja, S. Sharma, K. Ali, F. Bai, and A. F. Molisch, "Bistatic vehicular radar with 5G-NR signals," in 2023 IEEE Globecom, 2023, pp. 1034–1039.
- [15] Stadt Wien ViennaGIS. [Online]. Available: www.wien.gv.at/viennagis
- [16] A. F. Molisch, F. Tufvesson, J. Karedal, and C. F. Mecklenbräuker, "A survey on vehicle-to-vehicle propagation channels," *IEEE Wireless Communications*, vol. 16, no. 6, pp. 12–22, Dec. 2009.
- [17] S. Zelenbaba, M. Hofer, D. Löschenbrand, G. Kail, M. Schiefer, and T. Zemen, "Spatial properties of industrial wireless ultra-reliable lowlatency communication MIMO links," in 2019 53rd Asilomar Conference on Signals, Systems, and Computers, 2019, pp. 1054–1058.
- [18] G. Matz, "On non-WSSUS wireless fading channels," *IEEE Trans. Wireless Commun.*, vol. 4, no. 5, pp. 2465–2478, Sep. 2005.
- [19] L. Bernadó, T. Zemen, F. Tufvesson, A. F. Molisch, and C. F. Mecklenbrauker, "Delay and Doppler spreads of nonstationary vehicular channels for safety-relevant scenarios," *IEEE Trans. Veh. Technol.*, vol. 63, no. 1, pp. 82–93, Jan. 2014.
- [20] A. Paier, T. Zemen, L. Bernadó, G. Matz, J. Karedal, N. Czink, C. Dumard, F. Tufvesson, A. F. Molisch, and C. F. Mecklenbräuker, "Non-WSSUS vehicular channel characterization in highway and urban scenarios at 5.2 GHz using the local scattering function," in 2008 International ITG Workshop on Smart Antennas, Feb. 2008, pp. 9–15.
- [21] T. Zemen, C. Mecklenbräuker, F. Kaltenberger, and B. Fleury, "Minimum-energy band-limited predictor with dynamic subspace selection for time-variant flat-fading channels," *IEEE Trans. Signal Process.*, vol. 55, no. 9, pp. 4534–4548, Sep. 2007.